Comparing Hydrogen and Jet-A for an N+3 Turbofan with Water Recirculation using Gradient-Based Optimization

Peter N. Atma*, Andrew H .R. Lamkin†, and Joaquim R. R. A. Martins‡
University of Michigan, Ann Arbor, MI, 48109

Advances in commercial propulsion technology led to the development of efficient high bypass ratio turbofan engines with larger overall pressure ratios and internal temperatures. Current trends suggest that geared ultra high bypass ratio turbofans are the next generation of commercial propulsion systems. Furthermore, the emphasis on decreasing emissions has driven the exploration of hydrogen-powered aircraft, adding to the already challenging design space. Carrying and burning hydrogen introduces complexity and weight penalties that we must offset using the fuel's thermodynamic and chemical properties. In this study, we create a closed-loop water recirculation system with a zero-dimensional thermodynamic model and compare the benefits between jet-A and hydrogen fuels. We perform a gradient-based optimization parameter sweep to explore the trade-offs between performance and emissions using both fuels with water recirculation. The results quantify the design space for next-generation propulsion concepts that can take advantage of hydrogen fuel's advantageous thermodynamic properties to reduce emissions and improve performance.

I. Introduction

The effects of climate change are pushing the aviation industry towards hydrogen-fueled propulsion systems as a solution to reduce emissions. N+3 technology estimates for engines that burn hydrocarbon fuels suggest that higher efficiency can be achieved by designing ultra high bypass ratio (UHBR) turbofans with small cores and high overall pressure ratios (OPR). Higher OPR and smaller cores challenge the limits of compressor and turbine design, placing an upper bound on potential performance and emissions improvements. Switching to hydrogen as the primary fuel source reduces carbon dioxide emissions immediately, but adds complexity and weight that offset the benefits. However, hydrogen is a versatile fuel with advantageous molecular and thermodynamic properties that can be exploited to increase the performance and reduce emissions. We introduce a closed-loop water recirculation model that demonstrates the possible efficiency gain when hydrogen is used for purposes other than combustion.

Water injection is the process of introducing water upstream of the combustor as finely atomized droplets. NASA, Boeing, and Rolls-Royce studied this concept and suggested that this technique reduces the NOx emissions as much as 47 percent [1]. Additionally, water injection improves fuel efficiency and thrust output with lower combustion temperatures that can improve the lifetime of turbine blades and reduce noise [1]. Traditional propulsion systems that burn hydrocarbon fuels would require external water storage on the aircraft for water injection [2]. The added weight of tanks, pumping, and ducting makes this concept infeasible for a conventional aircraft. The main product of hydrogen combustion is water vapor that we can recover from the exhaust stream [3]. Condensing water vapor from the exhaust stream of hydrogen combustion and recirculating it eliminates any additional storage requirements. This allows for the theoretical design of a closed loop water feedback system inside the propulsion cycle. Pratt and Whitney are actively researching this technology to improve the feasibility of hydrogen-powered propulsion *.

Zero-dimensional cycle modeling is an efficient tool for predicting the initial design, performance, and emissions of new propulsion concepts. Zero-dimensional analysis uses a first-principles approach with a chemical equilibrium analysis (CEA) thermodynamics solver [4] that considers the molecular species of different fuels. The industry standard for thermodynamic cycle analysis is the Numerical Propulsion System Simulation (NPSS) framework [5]. NPSS is a modular object-oriented library that models engine components as individual blocks with several thermodynamic solvers. Hendricks and Gray [6] created a new tool called pyCycle with the same functionality as NPSS with analytical

*MSE Student, Department of Aerospace Engineering, AIAA Student Member
†Ph.D. Candidate, Department of Aerospace Engineering, AIAA Student Member
‡Professor, Department of Aerospace Engineering, AIAA Fellow

*https://arpa-e.energy.gov/technologies/projects/hydrogen-steam-and-inter-cooled-turbine-engine-hysite derivatives [7]. pyCycle is built on top of the OpenMDAO framework [8] to enable gradient-based optimization and leverage hierarchical nonlinear solver structures for robustness.

In this work, we analyze the thermodynamic benefits of a closed-loop water vapor recovery and water injection system in a high-bypass turbofan engine. We develop pyCycle components for water injection and vapor recovery to quantify the benefit of a closed loop recirculation system. We use gradient-based optimization to minimize fuel burn subject to performance requirements using both jet-A and hydrogen at a range of flight conditions. The optimized results show the trade-off between complexity, performance, and efficiency for jet-A and hydrogen fuels.

This work is organized as follows. First, in Section II, we introduce the turbofan model and explain the water injection and water recovery components. In section III the implementation of the multipoint optimization problem is discussed. Finally, we present the optimized results and discuss the design space in section IV.

II. Methodology

The UHB turbofan model is the NASA advanced technology "N+3" engine [9]. The N+3 reference cycle is a UHB ratio geared turbofan that could be available in the 2030 to 2040 time frame. The flow path consists of an inlet that directs ambient air through a fan, followed by a duct that splits the flow into a core and a bypass stream, each ending in a core and bypass nozzle, respectively. The low pressure system is split into two mechanical subsystems. First, the fan is connected to the gearbox that reduces the shaft speed to decrease fan tip speeds. Second, the gearbox attaches to the low-pressure shaft that connects to the low-pressure compressor (LPC) and low-pressure turbine (LPT). The high pressure compressor (HPC) is connected to the high pressure turbine (HPT) by the high pressure shaft.

We introduce the closed-loop water recovery system as a feedback cycle that transports water from the exhaust to upstream of the compressors. The recovery system injects vaporized water into the core stream that reduces the combustion temperature due to heat absorption. The vapor recovery component is placed directly before the core nozzle to extract water from the exhaust and recycle it back to the injector.

In this section we present the full engine layout and provide details on the multipoint zero-dimensional modeling approach. We explain the implementation and assumptions of the water recovery model and the coupling with the thermodynamic cycle.

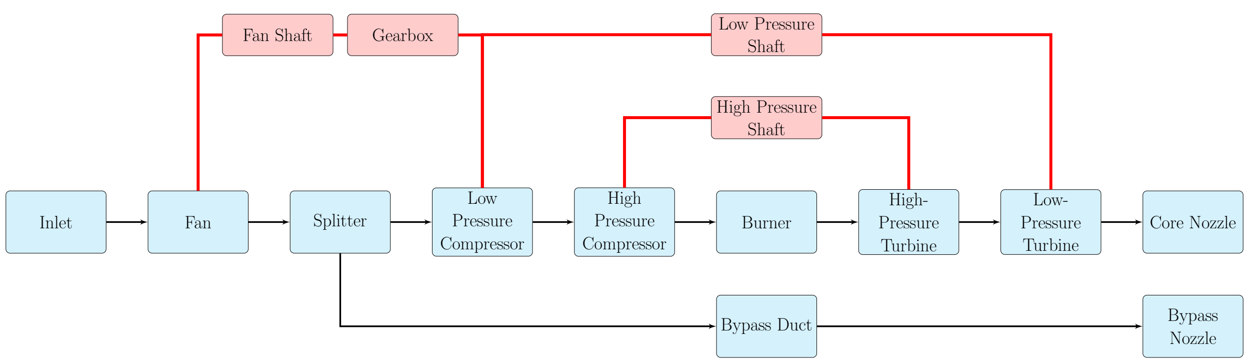

Fig. 1 Simplified layout of the N+3 engine cycle, adapted from Hendricks and Gray [6]. Black arrows are flow connections, red lines are mechanical connections, blue boxes are cycle elements, red boxes are shaft elements.

A. Water Recovery Model

We implemented the closed-loop water recovery system as a feedback cycle that extracts water from the exhaust stream and injects it upstream of the HPC. We chose this injection location based on claims from a study by NASA, Boeing, and Rolls-Royce [1] that water injection directly into the combustor is unnecessary. The water vapor recovery component sits downstream of the LPT and extracts water from the flow before exiting the core nozzle. We assume that a fraction of the total water available in the exhaust stream is recovered and that there are no pressure or temperature losses associated with this process. The component flow interface and mechanical connections, including the water injector and water extractor, are depicted in Figure 2.

To account for the humidity of the inlet air as well as the increased humidity after water injection, we modified the composition of the air mixture upstream of the combustor. pyCycle provides a `wet-air` dataset that introduces H_2O

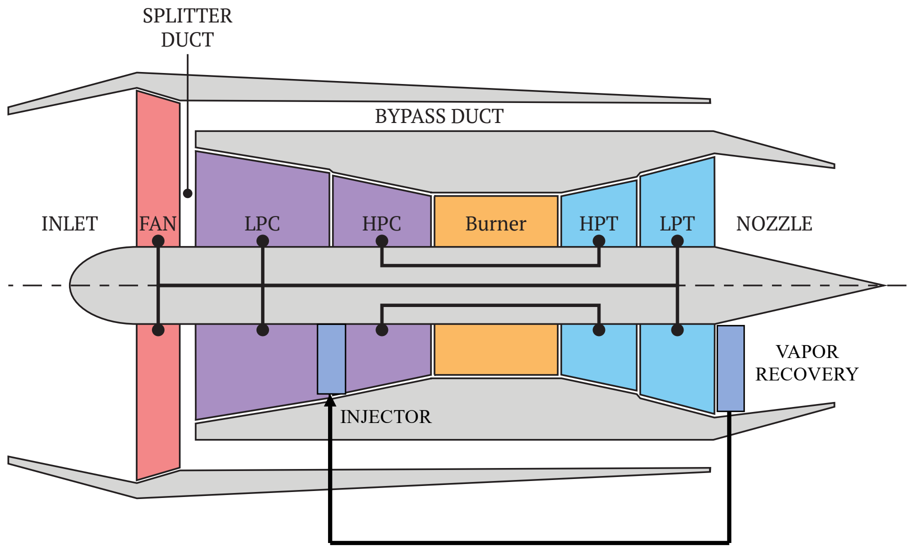

Fig. 2 The configuration of a high-bypass turbofan model with an integrated closed-loop water vapor recovery and injection system. The water vapor recovery system (extractor) extracts a fraction of the water in the core stream and reinjects it upstream of the high-pressure compressor. This diagram illustrates the feedback effect that this implementation has on the overall core flow.

molecules to the composition of air. We prescribe atmospheric mass-specific humidity as a water-to-air ratio (WAR) that is defined as the ratio of H_2O to air in the reactants of the inflow mixture. Kalnay et al. [10] give the humidity values for each flight condition.

We introduce two new thermodynamic models for water recirculation in pyCycle. A water injector adds water to the flow upstream of the HPC, while a water extractor diverts a portion of the water in the flow away from the exhaust stream. The injector operates similarly to fuel injection in the pyCycle combustor component. We determine a WAR that is analogous to the fuel-to-air (FAR) ratio in the combustor. This WAR is used to compute the chemical species present in the flow at the current thermodynamic state, determined by the incoming flow. The new species composition and thermodynamic state are determined using the pyCycle CEA solver [7]. The water injector inputs are the mass flow rate and mass fraction of water. We can solve for the mass flow rate on a mixture basis using the WAR, or directly by specifying the mass flow rate of water. A schematic of the injector is shown in Figure 3a where Y_{H_2O} is the mole fraction of water molecules.

The water extractor model diverts a fraction of a specific species from one flow path to another. The CEA solver calculates the inflow composition and the extractor separates a specific species based on a mass fraction input. The composition of the core stream is updated to represent the remaining mixture after the extractor model removes the species from the incoming flow. We then solve for the thermodynamic state and flow path areas at the outflow of both extractor streams. A simple schematic of the extractor is shown in Figure 3b where Y_{H_2O} is the mole fraction of water molecules and X_{H_2O} is the fraction of water that is recovered from the core stream.

We connect one outflow stream of the extractor to the inflow stream of the injector to complete the water recirculation system. The model results in a mismatch between the mass flow rate upstream of the HPC and the mass flow rate exiting the core nozzle. To preserve conservation of mass, we treat the water recirculation as a nonlinear cycle that must converge before the engine calculation is physically balanced. In this model, we are assuming the water molecules are removed from the exhaust stream with no pressure or temperature losses. We also assume the injected water molecules are at the same pressure and temperature as the air flow just before the HPC. We illustrate the water recirculation loop and the nonlinear solver connections in Figure 5.

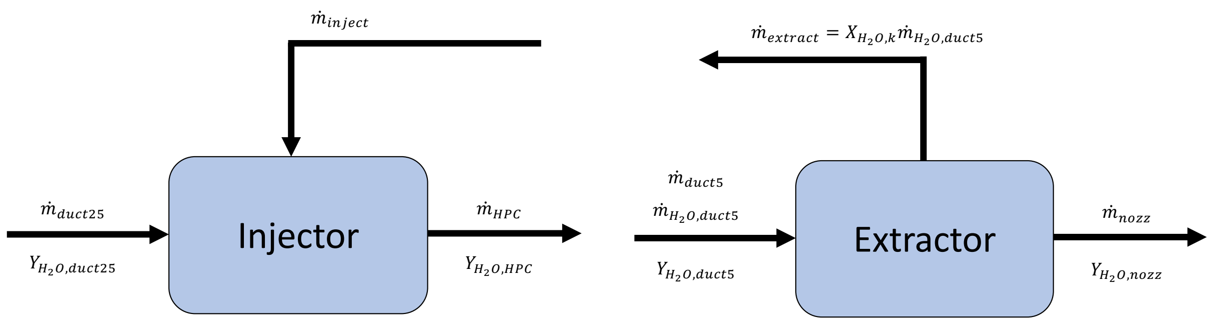

(a) Water from the extractor is simply injected into the core flow upstream of the high-pressure compressor.

(b) We extract a fraction of the moles of water from the out flow of duct 5. The extracted water is routed back upstream to the injector and the rest is exhausted out the nozzle.

Fig. 3 Injector (left) and extractor(right) diagrams that show the inputs and output streams of each component.

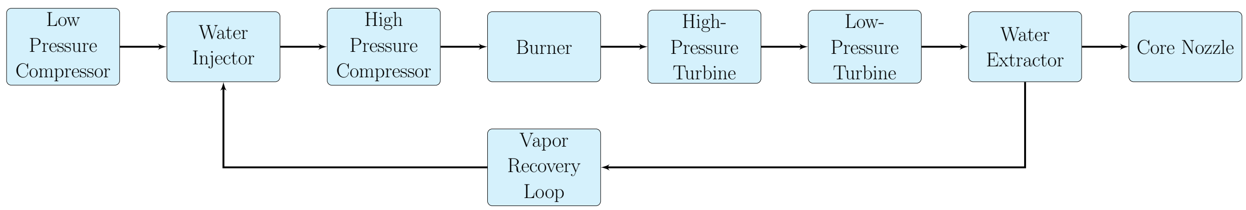

Fig. 4 Simplified layout of the N+3 engine cycle with the closed-loop vapor recovery. Black arrows are flow connections, red lines are mechanical connections, blue boxes are cycle elements, red boxes are shaft elements.

B. Multipoint Propulsion Model

The N+3 model is a collection of components that combine to form a unified zero-dimensional cycle. The model consists of twenty-five different elements that define the flow path and the mechanical systems. Thermodynamic quantities are solved and exchanged using CEA at flow path boundaries represented by black arrows between blue flow path components in Figure 1. The fan, gearbox, low pressure, and high pressure systems are connected by three mechanical shafts depicted in red in Figure 1.

We operate the engine cycle in different modes depending on the desired conservation relationships, design rules, and flight conditions. In "on-design" mode, we prescribe cycle inputs such as turbo machinery efficiencies, pressure ratios, and combustion temperatures. The "off-design" mode inherits the flow path areas and turbo machinery map scalars from the "on-design" analysis.

We impose *balance* equations to satisfy the physical governing equations, conservation laws, and design rules. *Balance* relationships are formulated as equations in the form $r(u) = 0$ where r is a residual function and u is an implicit state variable. We use Newton based solvers to find the value of the state variables that drive the set of balance residuals to zero. Hendricks and Gray provide the extensive set of balance equations with further details on the construction of the nonlinear system for the N+3 model.

Table 1 Altitude and mach numbers at each of the flight conditions considered in the multipoint formulation.

Parameter	TOC	RTO	SLS	CRZ	Units
Altitude	35000	0	0	35000	ft
Mach	0.8	0.25	0.0	0.8	-
Humidity Ratio	0.00017	0.009	0.009	0.00017	kg/kg

The "on-design" point is top-of-climb (TOC) with "off-design" conditions at rolling takeoff (RTO), sea-level static (SLS), and cruise (CRZ). Table 1 shows the different altitudes and mach numbers for each flight condition. We consider these points because they either limit the performance at cruise or present critical design considerations for the propulsion system. The design rules at SLS ensure that the turbo machinery and flow paths meet the static thrust target. Rolling takeoff limitations constrain the upper limit of the combustor temperature and subsequently the cooling requirements of the turbines. The cooling mass flow rates ($\dot{m}_{\mathrm{cool,k}}$) are passed from the RTO point to all other flight conditions creating a cyclic connection. We add a fuel burn objective at cruise to optimize the engine performance during the longest flight segment. We size the water recovery system at the CRZ condition because it has the greatest impact on fuel burn over the flight envelope. Similarly to $\dot{m}_{\mathrm{cool,k}}$, the water recovery mass flow rates ($\dot{m}_{\mathrm{water,k}}$) are connected back to the other operating points. The interconnections between flight conditions create a complex nonlinear loop, shown in Figure 5. The converged model represents a feasible multipoint engine that accounts for design considerations at all four operating conditions. We direct the reader to the N+3 multipoint model definition in the paper by Hendricks and Gray [6] for the detailed description of the balance relationships.

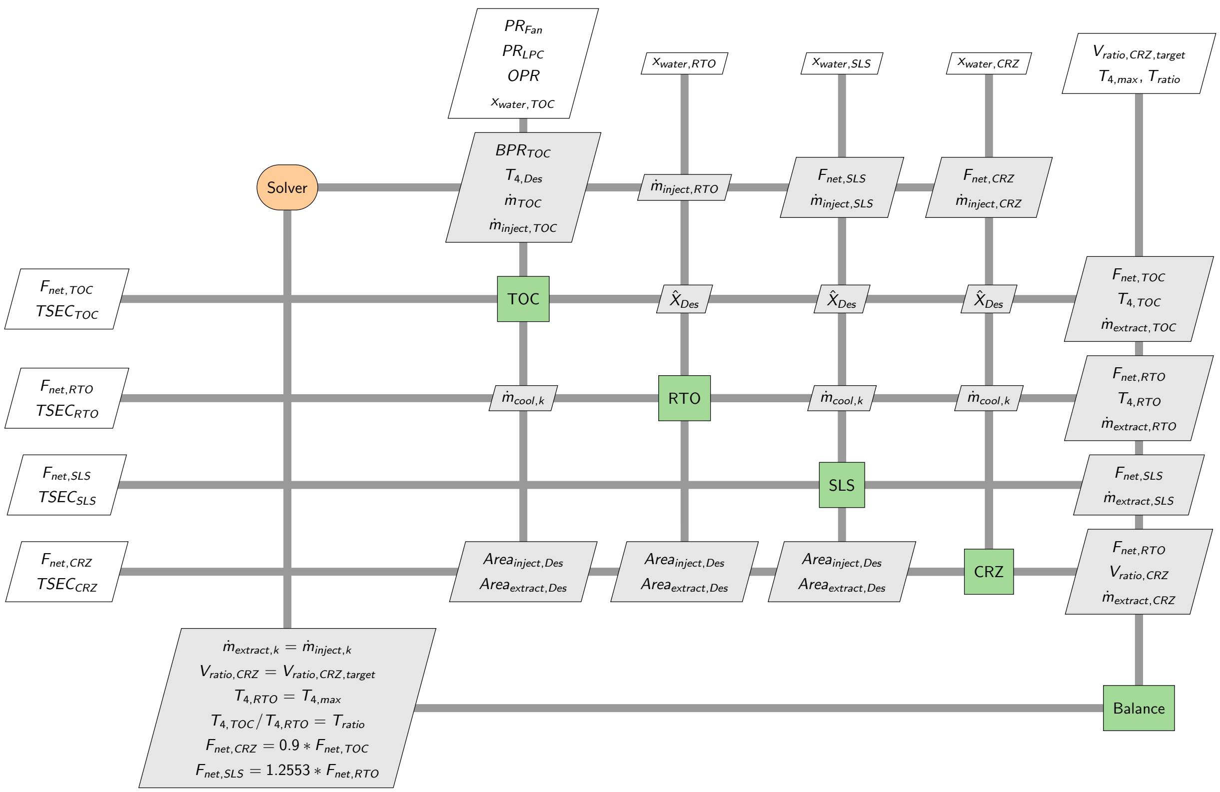

Fig. 5 Full multidisciplinary design analysis (MDA) model N+3 XDSM diagram. This XDSM diagram shows the multipoint coupling between the different operation conditions and shows how the water recovery fractions are used to solve for water mass flow rates.

III. Optimization Problem

We performed multipoint gradient-based design optimization of the N+3 engine model considering the TOC, RTO, SLS, and CRZ flight conditions. The objective is to minimize fuel burn subject to design and performance constraints.

Typical gas-turbine analysis measures the efficiency using the thrust-specific fuel consumption (TSFC). However, this metric is not useful in the comparison of efficiency between jet-A and hydrogen fueled cycle models because of the differences in fuel density and energy capacity. A better metric for comparing Jet-A versus hydrogen is thrust-specific energy consumption (TSEC). TSEC is TSFC multipied by the lower heating value (LHV) of the fuel shown in Equation (2).

$$\mathrm{TSFC} = \frac{\dot{m}_{\mathrm{fuel}}}{F_{\mathrm{thrust}}} \tag{1}$$

$$\mathrm{TSEC} = \frac{\dot{m}_{\mathrm{fuel}}\mathrm{LHV}}{F_{\mathrm{thrust}}} = \mathrm{TSFC} \times \mathrm{LHV} \tag{2}$$

Therefore, TSEC at the cruise condition is the objective function in the optimization problem. An XDSM diagram of the optimization problem with the multipoint formulation is shown in Figure 6.

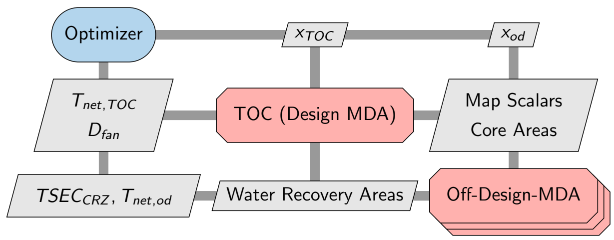

Fig. 6 XDSM diagram of the multipoint optimization problem with objective, constraints, and MDA block. The XDSM diagram shows the variables and outputs within the optimization model and how each of these values is connected to the optimizer and MDA block.

The design variables for this problem are water recovery fraction at CRZ ($X_{\mathrm{H_2O,CRZ}}$), fan pressure ratio ($\mathrm{PR}_{\mathrm{fan,TOC}}$), low pressure compressor pressure ratio ($\mathrm{PR}_{\mathrm{LPC,TOC}}$), overall pressure ratio at CRZ ($\mathrm{OPR}_{\mathrm{TOC}}$), burner temperature at RTO ($T_{4,\mathrm{RTO}}$), TOC-RTO burner temperature ratio ($T_{4,\mathrm{ratio}}$), and the nozzle velocity ratio at CRZ ($V_{\mathrm{ratio,CRZ}}$). Only the water recovery fraction at CRZ is a design variable since we are optimizing $\mathrm{TSEC}_{\mathrm{CRZ}}$. TOC-to-RTO burner temperature ratio ($T_{4,\mathrm{ratio}}$) is shown in Equation (3).

$$T_{4,\mathrm{ratio}} = \frac{T_{4,\mathrm{TOC}}}{T_{4,\mathrm{RTO}}} \tag{3}$$

This optimization problem was run for both Jet-A and H2 fuels using the fuel properties in 2 and flight conditions in Table 1. The optimization problem objective function, design variables, and constraints are shown in Table 3 below.

Table 2 N+3 model fuel properties. The lower heating values are given for each fuel used to compute TSEC.

Parameter	Value	Units	Description
$\mathrm{LHV}_{\mathrm{JetA}}$	18564.0	BTU/lbm	Lower heating value of Jet-A †
$\mathrm{LHV}_{\mathrm{H2}}$	51591.0	BTU/lbm	Lower heating value of H2 ‡

The N+3 pyCycle model is implemented in OpenMDAO [8] to enable multidisciplinary gradient-based optimization with analytic coupled derivatives. We use pyOptSparse [11] to facilitate the use of state-of-the-art optimization software through a unified python interface. We solve the optimization problem listed in Table 3 with SNOPT [12], a gradient-based sequential quadratic programming (SQP) algorithm for large-scale constrained problems.

IV. Results

Our fuel performance metric is TSEC but minimizing $\dot{m}_{fuel}$ is a better posed optimization problem since we will also have thrust constraints. Therefore, the fuel flow rate at CRZ, $\dot{m}_{fuel,CRZ}$, was set as the objective.

When $T_{4,\mathrm{RTO}}$ and $X_{\mathrm{H_2O,CRZ}}$ are design variables at the same time it was found that the optimizer pushes $T_{4,\mathrm{RTO}}$ down and $X_{\mathrm{H_2O,CRZ}}$ up. Since these two variables are at odds with each other and the upper limit for $X_{\mathrm{H_2O,CRZ}}$ is where the model breaks, $T_{4,\mathrm{RTO}}$ was set as the optimal value from the optimizations with no water recirulation. The upper bound on $X_{\mathrm{H_2O,CRZ}}$ was found to be around 30% for Jet-A and 17% for H2.

The 4 optimizations mentioned in the section III were run and solved. The optimality, feasibility, and merit function for each optimization is shown plotted in Figure 7.

Table 3 Multipoint optimization problem definition. The objective function is the thrust specific energy consumption at the cruise condition. The constraints are net thrust and engine diameter constraint at the design point, TOC.

	Variable/Function	Description	Units	Quantity
minimize	$\mathrm{TSEC_{CRZ}}$	Thrust-specific energy consumption at CRZ (Equation (2))	lbm/s	1
with respect to	$X_{\mathrm{H_2O,CRZ}}$	Water recovery fraction at CRZ	-	1
	$\mathrm{PR_{fan,TOC}}$	TOC fan pressure ratio	-	1
	$\mathrm{PR_{LPC,TOC}}$	TOC low-pressure compressor pressure ratio	-	1
	$\mathrm{OPR_{TOC}}$	TOC overall pressure ratio	-	1
	$T_{4,\mathrm{RTO}}$	RTO combustor temperature	°R	1
	$T_{4,\mathrm{ratio}}$	TOC-to-RTO temperature ratio (Equation (3))	-	1
	$V_{\mathrm{ratio,CRZ}}$	Core-to-bypass nozzle velocity ratio at CRZ (Equation (**??**))	-	1
		Total		7
subject to	$F_{\mathrm{net,TOC}} \geq 5800.0$	Target net thrust at TOC	lbf	1
	$D_{\mathrm{fan}} \leq 100$	Maximum Fan Diameter	inch^2	1
		Total		2

Table 4 Design variable ranges for the optimization problem.

Design Variable	Lower	Upper	Units
$x_{H2O,CRZ}$	0.0	-	-
$PR_{fan,TOC}$	1.2	1.4	-
$PR_{LPC,TOC}$	2.5	4.0	-
$PR_{OPR,TOC}$	40.0	70.0	-
$T_{4,TOC}/T_{4,RTO}$	0.5	0.95	-
$T_{4,RTO}$	3000.0	3600.0	°R
$V_{ratio,CRZ}$	1.35	1.45	

From this plot we can visually check that each optimization achieved optimality and feasibility, and that the merit function reached a steady-state value. Indeed, we observe quadratic convergence in the optimality of the problem near the optimal solution as expected. The design variable history for each optimization problem is shown in Figure 8.

From this figure we see that the design variables start at the initial values and converge toward their optimal value. Note that the $T_{4,\mathrm{RTO}}$ variables are only present for the optimizations without water recovery and the $X_{\mathrm{H_2O,CRZ}}$ variables are present only for the optimizations with water recovery. The constraint history for each optimization problem is shown in Figure 9.

From this figure we can see that the constraints are quickly satisfied and for the most part remain feasible for the duration of the optimization. The resulting optimal values from the optimization problems are shown in Figure 10 on a parallel coordinate plot.

We can see that the resulting engine designs are all very similar. The main differences in the engine designs are the pressure ratios and temperatures. Between the two fuel types, the water recovery fraction for both is pushed up to the upper limit of the design space. The recovery fraction does not directly relate to the mass flow rate of recirculated water. The recovery fraction for H_2 is smaller than the recovery fraction for jet-A because there is more water produced in the combustion process. However, the mass flow rate of water is larger for H_2 at 0.405 lbm/s as opposed to 0.324 lbm/s for jet-A. The H_2 has the benefit of recovering more water at a lower fraction of the overall water in the core exhaust. We see slightly higher pressure ratios across the fan with water recovery leading to a larger overall pressure ratio. The LPC pressure ratio tend to the upper bound for each optimization with and without water recovery enabled. The $T_{4,\mathrm{RTO}}$ value for Jet-A is slightly higher than that of H2. Furthermore, adding water recovery slightly decreases the $T_{4,\mathrm{ratio}}$

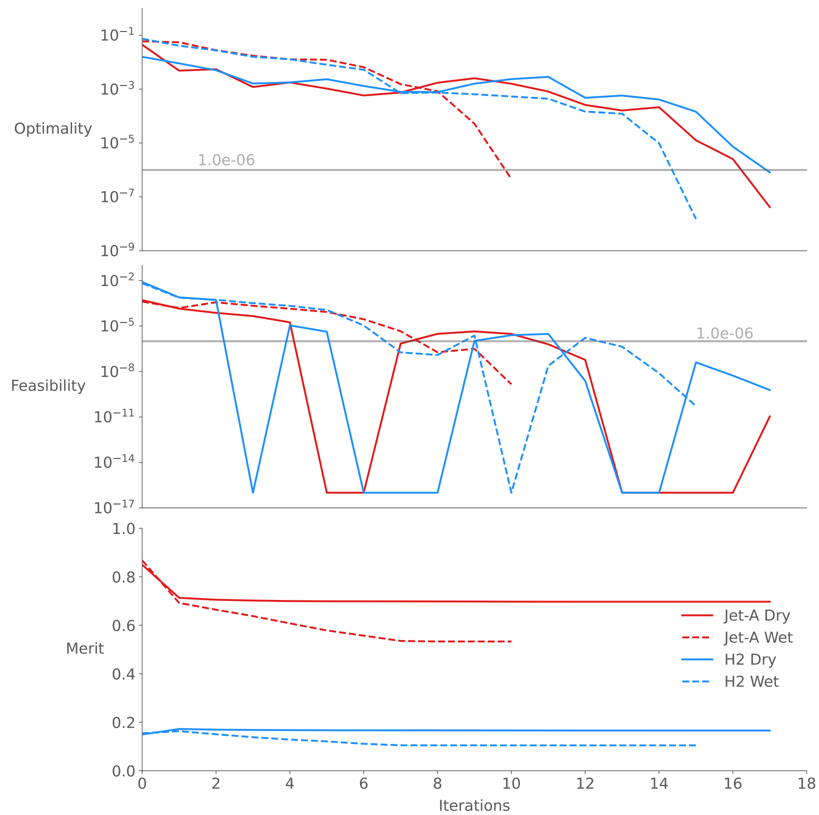

Fig. 7 The optimality, feasibility, and merit fuction history for each optimization problem. Jet-A without water recovery is shown with the solid lines, the Jet-A with water recovery is shown with dashed lines, hydrogen without water recovery is shown with dash-dot lines, and hydrogen with water recovery is shown with dotted lines.

value. Therefore, temperatures are cooler with the H_2 fuel and even slightly cooler when adding water recovery. It is noted that with more water recovery the farther the optimizer would push the value of $T_{4,\mathrm{RTO}}$ down. Therefore, there are temperature-related advantages of using water recovery to maintain a certain effenciency and thrust. The breakdown of thrust for each point is shown in Table 5. This table shows the resulting net thrust, gross thrust, and ram drag of each engine design for the four optimizations performed.

From this table we can see that the net thrust is constrained at values set by *balance* components or optimization constraints.

Given that most of the design variables change only slightly between designs, most of the efficiency gains are driven by water injection. In fact, we can see the $\mathrm{TSEC}_{\mathrm{CRZ}}$ improvement due to water recovery relative to no water recovery for both fuels in Figure 11.

Based on this analysis and model, we see an improvement greater than 5% at CRZ for TSEC for both fuels. This level of improvement would have a significant reduction in fuel costs over the course of an engine's lifecycle. Due to the comparatively small amount of water in the exhaust stream for Jet-A, the Jet-A engine would require a larger condenser [3]. Therefore, H_2 is a much more appealing fuel to use with the proposed closed-loop water recovery system. Since there is a lack of literature on large-scale water condensers that are designed to fit inside a turbofan engine, a relatively low pressure loss condenser would need to be developed for this system to work. Given the lack of knowledge of the type of condenser that would need to be require, we performed a pressure loss sweep of the H2 engine. pyCycle handles pressure losses in ducts by specifying a pressure loss coefficient, dPqP. This coefficient is the ratio of change in total pressure normalized by the inlet pressure of the duct. The pressure loss of the duct just upstream of the extractor was varied while the rest of the engine design variables were optimized. Figure 12a shows $\mathrm{TSEC}_{\mathrm{CRZ}}$ of this sweep relative to and engine with no water recovery.

From this figure, we can see the design area in which the closed-loop water recovery model is beneficial. This model will offer efficiency benefits up until about dPqP = 0.16 which means a 16% loss of pressure from the condenser. This

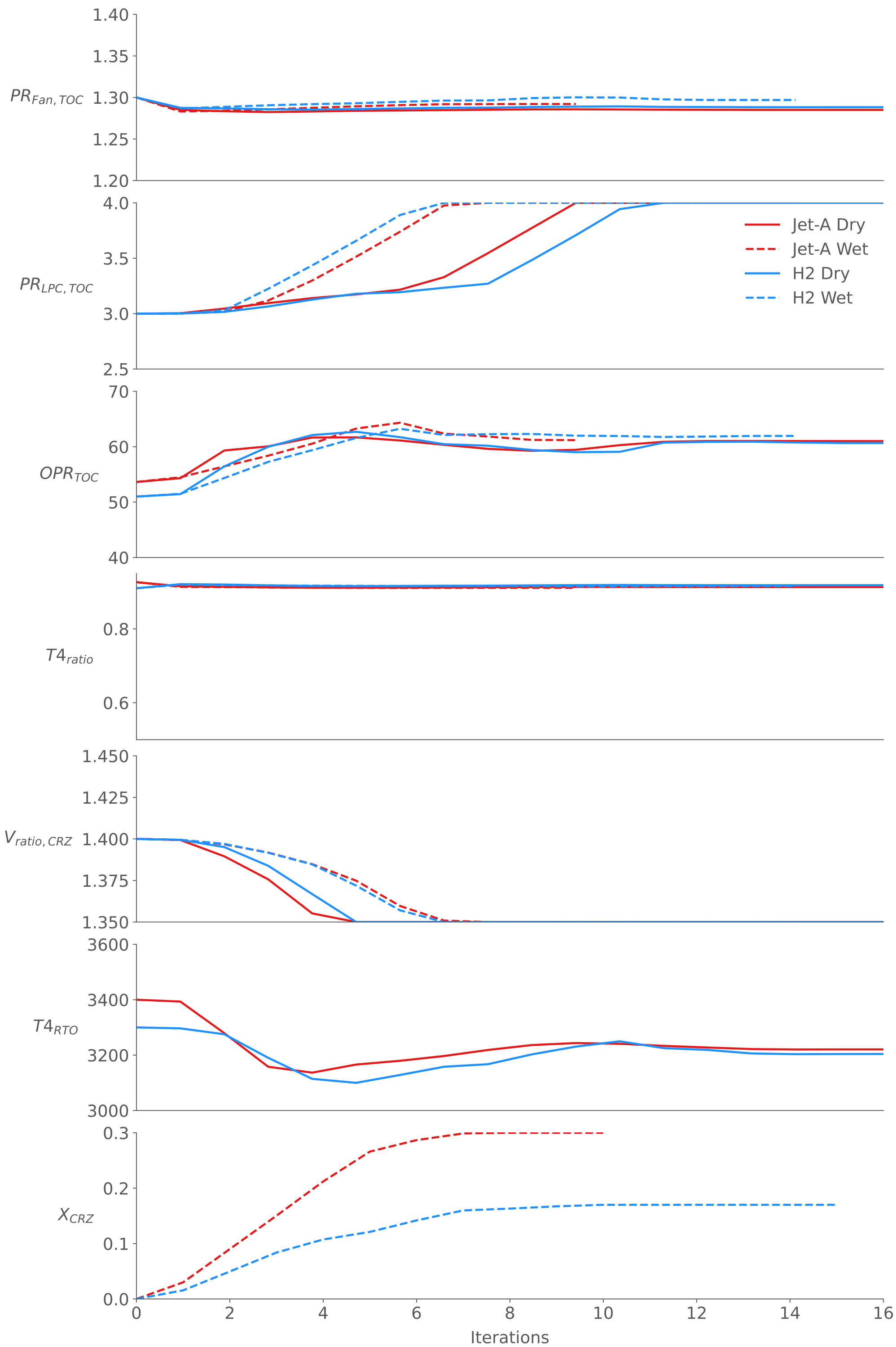

Fig. 8 The design variable history for each optimization problem. Jet-A without water recovery is shown with the solid lines, the Jet-A with water recovery is shown with dashed lines, hydrogen without water recovery is shown with dash-dot lines, and hydrogen with water recovery is shown with dotted lines.

benefit area would be reduced if a smaller fraction of water recovered could be obtained. Figure 12b shows the total

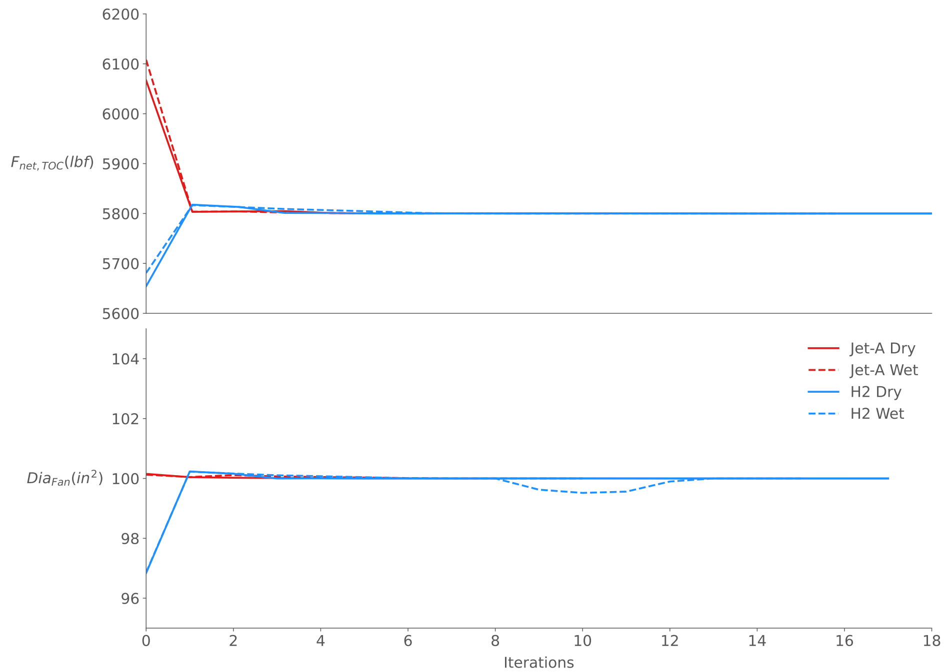

Fig. 9 The constraint history for each optimization problem. Jet-A without water recovery is shown with the solid lines, the Jet-A with water recovery is shown with dashed lines, hydrogen without water recovery is shown with dash-dot lines, and hydrogen with water recovery is shown with dotted lines.

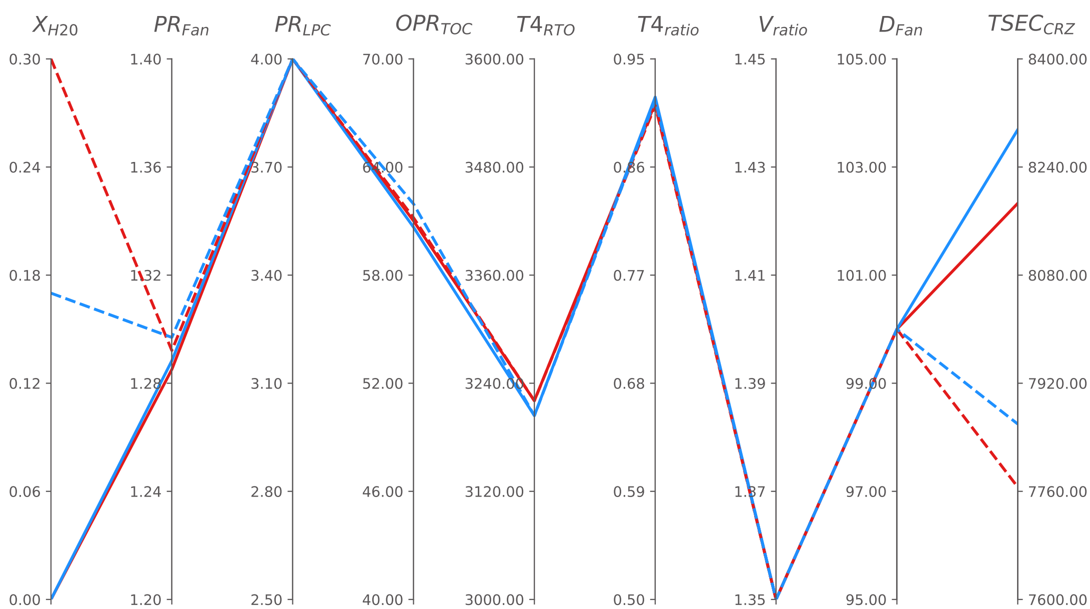

Fig. 10 Optimization results of the N+3 engine with and without no water recovery using Jet-A and H2 as the fuel. The red lines show Jet-A fuel and the blue lines show H_2 fuel. The solid lines show the engine without water recovery and the dashed lines show the engine with water recovery.

Table 5 Thrust breakdown for each flight operating condition. The net thrust, gross thrust, and ram drag are shown for each optimization result.

Point	Parameter	Jet-A Dry	Jet-A Wet	H2 Dry	H2 Wet
TOC	Net Thrust, lbf	5800.0	5800.0	5800.0	5800.0
	Ram Drag, lbf	19623.4	19623.4	19623.4	19623.4
	Gross Thrust, lbf	25423.4	25423.4	25423.4	25423.4
RTO	Net Thrust, lbf	22800.0	22800.0	22800.0	22800.0
	Ram Drag, lbf	17089.7	17043.5	17070.8	17014.6
	Gross Thrust, lbf	39889.7	39843.5	39870.8	39814.6
SLS	Net Thrust, lbf	28620.8	28620.8	28620.8	28620.8
	Ram Drag, lbf	61.8	61.7	61.8	61.6
	Gross Thrust, lbf	28682.7	28682.5	28682.6	28682.4
CRZ	Net Thrust, lbf	5220.0	5220.0	5220.0	5220.0
	Ram Drag, lbf	19194.0	19152.9	19190.3	19144.1
	Gross Thrust, lbf	24414.0	24372.9	24410.3	24364.1

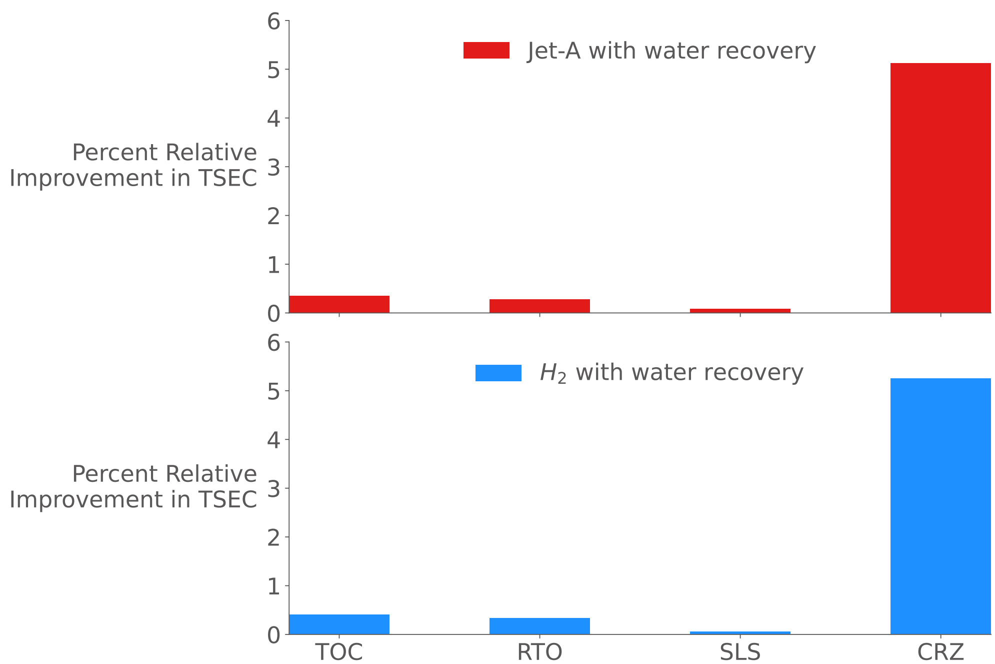

Fig. 11 Percent relative improvement in thrust specific energy consumption (TSEC) of the N+3 engine with water recovery. This plot compares the relative improvement of the two optimization problems with water recovery compared to the optimization problems without water recovery.

water available in the core stream as a function of the same pressure loss.

This figure shows that the optimizer finds designs that increase the available water in the core stream. Since the water recovery fraction is always pushed to 17%, the water recovered is increased to overcome the pressure loss. This effect helps the engine increase the benefit area in Figure 12a.

V. Conclusion

In this paper, we describe a how a novel closed-loop water recirculation system would be integrated in a commercial aviation setting. The water recirculation system comprised was designed and implemented into the N+3 ultra-high

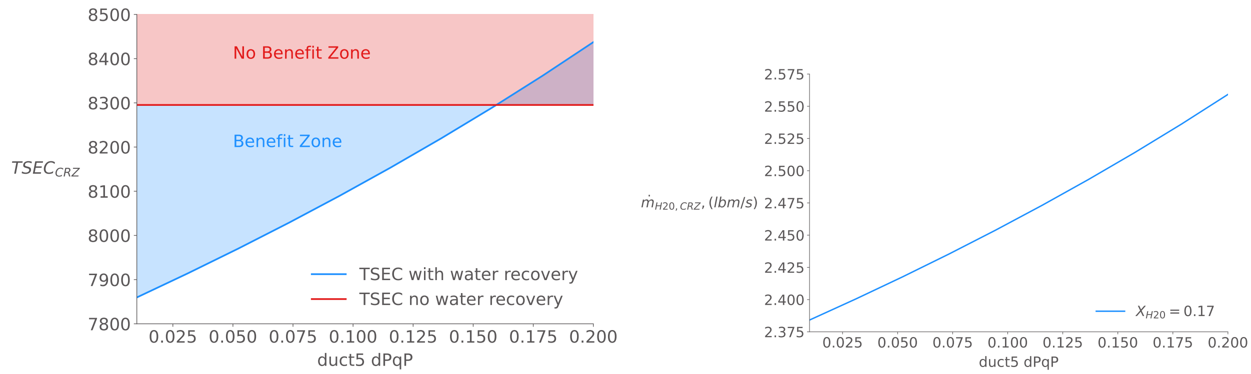

(a) Pressure loss sweep of Duct5 which is just upstream of the water vapor extractor component. The figure shows the optimized TSEC values for varying levels of pressure loss due to the condensation of water compared to the optimization problem without water recovery. This shows the working space available for designing a water condenser while still gaining the benefits of water recovery.

(b) Pressure loss sweep of Duct5 which is just upstream of the water vapor extractor component. The figure shows the resulting total available water in the exhaust stream for varying levels of pressure loss in the extractor flow path. The engine was optimized with the water recovery upper bound of 17%.

Fig. 12

bypass engine model. We have presented the results of four optimization problems demonstrating the use of this technology using the pyCycle cycle modeling tool for Jet-A and hydrogen fuel.

The recirculation system is implemented by introducing two new custom pyCycle components, the water extractor and injector, which form a continuous closed-loop feedback water flow in the engine. We then described the multipoint design problem and how it is used to design an aircraft engine to meet the operating requirements at different flight regimes. System-level *balance* constraints on the engine are described to show how a reduced-space optimization problem can be developed. The optimization problem is then introduced with constraints on the design point thrust and overall engine size with thermodynamic design variables describing the temperatures, presusres and velocities within the engine. An additional design variable controlling how much water is recirulated is added at the CRZ point to improve the fuel burn.

The results from the optimization problems show temperature, thrust, and efficiency improvements when using hydrogen as a fuel with water circulation. Thermal reductions will improve the lifetime of the engine which impact maintanence and overall costs. Between the two fuels, we see similar values of TSEC. Significant energy efficiency gains are seen with water recirculation and injection. This would lead to lower operating costs over the lifetime of the engine.

Technological problems do exist such as how to design a condensor that can recover a large portion of the exhaust water without large pressure losses. However, the thermal properties of hydrogen provide a heat sink and thus a readily available resource for condensation. Furthermore, using the exhaust stream to heat the hydrogen fuel has been proposed as an additional avenue to improve engine efficiencyThe results from this work outline the working space available for the design of such a condenser.

VI. Acknowledgements

References

[1] Daggett, D. L., Fucke, L., Hendricks, R. C., and Eames, D. J., "Water Injection on Commercial Aircraft to Reduce Airport Nitrogen Oxides," Tech. rep., NASA, March 2010.

[2] Mourouzidis, C., Igie, U., Pilidis, P., and Singh, R., "WATER INJECTION ON AIRCRAFT ENGINES: A PERFORMANCE, EMISSIONS AND ECONOMIC STUDY," 2015.

[3] Ström, L. J., and Gierens, K., "First simulations of cryoplane contrails." *Journal of Geophysical Research*, Vol. 107, 2002. doi:10.1029/2001JD000838.

[4] Gordon, S., and McBride, B. J., “Computer Program for Calculation of Complex Chemical Equilibrium Compositions, Rocket Performance, Incident and Reflected Shocks, and Chapman-Jouguet Detonations,” *NASA Rept. RP-1311*, 1994.

[5] Jones, S., *An Introduction to Thermodynamic Performance Analysis of Aircraft Gas Turbine Engine Cycles Using the Numerical Propulsion System Simulation Code*, NASA, 2007. TM-2007-214690.

[6] Hendricks, E. S., and Gray, J. S., “pyCycle: A Tool for Efficient Optimization of Gas Turbine Engine Cycles,” *Aerospace*, Vol. 6, No. 87, 2019. doi:10.3390/aerospace6080087.

[7] Gray, J. S., Chin, J., Hearn, T., Hendricks, E., Lavelle, T., and Martins, J. R. R. A., “Chemical Equilibrium Analysis with Adjoint Derivatives for Propulsion Cycle Analysis,” *Journal of Propulsion and Power*, Vol. 33, No. 5, 2017, pp. 1041–1052. doi:10.2514/1.B36215.

[8] Gray, J. S., Hwang, J. T., Martins, J. R. R. A., Moore, K. T., and Naylor, B. A., “OpenMDAO: An open-source framework for multidisciplinary design, analysis, and optimization,” *Structural and Multidisciplinary Optimization*, Vol. 59, No. 4, 2019, pp. 1075–1104. doi:10.1007/s00158-019-02211-z.

[9] Jones, S. M., Haller, W. J., and Tong, M. T., “An N+3 Technology Level Reference Propulsion System,” Tech. Rep. NASA/TM—2017-219501, NASA Glenn Research Center, 2017. URL `https://ntrs.nasa.gov/citations/20170005426`.

[10] Kalnay, E., Kanamitsu, M., Kistler, R., Collins, W., Deaven, D., Gandin, L., Iredell, M., Saha, S., White, G., Woollen, J., Zhu, Y., Chelliah, M., Ebisuzaki, W., Higgins, W., Janowiak, J., Mo, K. C., Ropelewski, C., Wang, J., Leetmaa, A., Reynolds, R., Jenne, R., , and Joseph, D., “The NCEP/NCAR 40-Year Reanalysis Project.” *Bulletin of the American Meteorological Society*, Vol. 77, 1996, pp. 437–471.

[11] Wu, N., Kenway, G., Mader, C. A., Jasa, J., and Martins, J. R. R. A., “pyOptSparse: A Python framework for large-scale constrained nonlinear optimization of sparse systems,” *Journal of Open Source Software*, Vol. 5, No. 54, 2020, p. 2564. doi:10.21105/joss.02564.

[12] Gill, P. E., Murray, W., and Saunders, M. A., “SNOPT: An SQP Algorithm for Large-Scale Constrained Optimization,” *SIAM Review*, Vol. 47, No. 1, 2005, pp. 99–131. doi:10.1137/S0036144504446096.